An Academic Adventure from the Transition Metal Nanocatalysts to the Non-Metallic Heterogeneous Photocatalysts on the Way to Development of Sustainable Chemical Transformations

By: Önder Metin, Melek Sermin Özer, Zafer Eroğlu

https://doi.org/10.51167/acm00063

The Emergence of Nanocatalysis: Catalysis plays an indispensable role in the chemical industry and serves as a vital pillar on which the entire structure of modern chemistry and manufacturing stands. Its importance lies in its ability to accelerate chemical reactions, optimize resource use, and improve product quality while reducing energy consumption and environmental impact, which are all among the sustainable development goals.[1–3] Without catalysis, the chemical industry as we know it would be very different, with inefficiencies, higher costs, and greater environmental damage. Among the types of catalysts used in industrial chemical transformations, heterogeneous catalysts are the preferred choice compared to homogeneous catalysts due to their advantageous properties such as ease of separation, reusability, and reduction of environmental impacts, which contribute to economic and environmental sustainability.[4–6] While heterogeneous catalysts offer many advantages, they suffer from their limited surface area, mass transfer limitations and low product selectivity.[7] All these problems can be overcome by reducing the size of heterogeneous catalysts to the nanoscale; This gives rise to a new class of catalysts called "hybrid" or "semi-heterogeneous" nanocatalysts, which combine the advantageous properties of homogeneous and heterogeneous catalysts.

Since transition metals are the most widely used catalysts in the chemical industry, transition metal nanoparticles (TMNPs), which have a considerably larger surface area and more catalytically active surface atoms than bulk metals, have attracted much attention over the past three decades.[8–10] They show advantageous catalytic properties compared to those of homogeneous and bulk heterogeneous analogs, and thus "*Nanocatalysis*" has been growing rapidly for several decades. To date, nanoparticles of all catalytically active transition metals have been synthesized using different methods, their catalysis in various reactions has been investigated, and many of them have even been patented and are commercially available in the catalogs of well-known chemical suppliers.[11] However, in the last decade, the interest in the use of bimetallic nanoparticles instead of monometallic ones has received great attention because the bimetallic NPs either in alloy or core-shell form generally show higher activity, selectivity and stability compared to the monometallic counterparts owing to the "*Synergistic*" effects (referring the geometric and electronic changes observed on the metals) formed between two distinct metal atoms.[12] In particular, economical yet efficient catalysts could be developed by the preparation of bimetallic alloy or core-shell NPs of noble metals with non-precious metals, which is considered to be very advantageous for catalytic reactions using noble metals as catalysts.[13–15] However, the composition control over the bimetallic nanoparticles is very important for the rational design of the most efficient catalysts in different catalytic applications, in which our research group, namely Metin Research Group (MRG) has enjoyed contributing to its progress and conceptual expansion. Our major achievements in the field of nanocatalysis over the last decade are the rational design and synthesis of monometallic and bimetallic nanoparticles (alloy or core-shell) as catalysts for various chemical transformations including hydrogen generation from the solid or liquid chemical hydrogen storage materials, C-C cross-coupling reactions and hydrogenations (**Figure 1**).[16–28] In the first part of this article, our most important studies about the synthesis of monodisperse mono/bimetallic nanoparticles and their catalytic applications in various chemical transformations are summarized.

Supported Monometallic Nanoparticles as Catalysts

Our group has synthesized many high-quality transition-metal NPs including Ni, Pd, Ru and Pt. The first monodisperse NPs synthesis that was done in our group was the monodisperse Ni NPs in 2010.[16] The Ni NPs were synthesized by the reduction of nickel(II) acetylacetonate ($Ni(acac)_2$) with borane-*tert*-butylamine (BTB) as a mild-reducing agent in the mixture of oleylamine (OAm) serving both as a solvent and surfactant and oleic acid (OA) as a co-surfactant. As-synthesized Ni NPs were then anchored on Ketjen Carbon (Ni/KC) via an ultrasound-assisted liquid phase self-assembly (ULPSA) method to be employed as a reusable catalyst. **Figure 1a and 1b** show the representative transmission electron microscopy (TEM) images of the colloidal Ni NPs and Ni/KC nanocatalysts, respectively. From the TEM images, it was concluded that colloidal Ni NPs possess a monodisperse particle size distribution with a size of 3.2 ± 0.2 nm and they preserve their morphology and particle size after their deposition on KC. After the detailed characterization studies, the Ni/KC nanocomposites were tested as catalysts in the hydrogen generation from the hydrolysis of ammonia borane (AB) for chemical hydrogen storage. The Ni/KC catalysts were highly active for hydrogen generation from the hydrolytic dehydrogenation of AB with a turnover frequency (TOF) of 792 mol H_2. (mol Ni)$^{-1}$.h^{-1} and even at low catalyst and substrate concentrations at room temperature. In a follow up study, we demonstrated that the catalytic activity of Ni NPs in the hydrolysis of AB could be further enhanced by depositing them on commercially available SiO_2, which revealed the support effect on the catalytic activity of the Ni NPs.[17]

Our successful results with monodisperse Ni and Pd NPs as catalysts in the hydrolytic dehydrogenation of AB prompted us to synthesize and investigate the catalytic of other catalytically active transition-metals such as Ru. Upon the great effort of my first Ph.D. student, Dr. Hasan Can, we achieved to synthesize nearly-monodisperse Ru NPs via tandem thermal decomposition and reduction of Ru(II) acetylacetonate ($Ru(acac)_3$) by OAm serving both as a surfactant and reducing agent in benzyl ether at 300 °C.[21] Since we could not separate the yielded ultra-small Ru NPs (2.5 nm) via the centrifugation process, we had to directly deposit them on the commercially available nano-Al_2O_3. After the separation from the synthesis mixture and the subsequent acetic acid treatment of the Ru/Al_2O_3 nanocatalysts, they were tested as catalysts in the hydrolysis of AB at room temperature and showed 2.5 and 6.3 times higher catalytic activity (TOF= 4998 mol H_2. (mol Ru)$^{-1}$.h^{-1}) than Pd/rGO and Ni/KC nanocatalysts, respectively.

Our above studies and other studies in the literature have revealed that noble metal NPs are more active catalysts in the hydrolysis of AB than first-row transition metals.[28–30] However, the practical use of noble metals as catalysts is limited due to

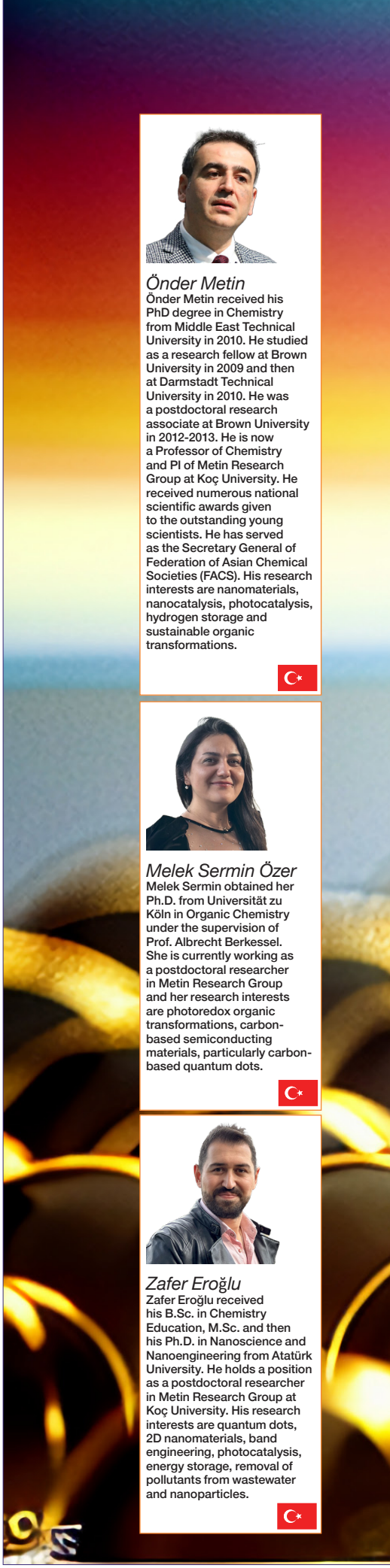

Önder Metin
Önder Metin received his PhD degree in Chemistry from Middle East Technical University in 2010. He studied as a research fellow at Brown University in 2009 and then at Darmstadt Technical University in 2010. He was a postdoctoral research associate at Brown University in 2012-2013. He is now a Professor of Chemistry and PI of Metin Research Group at Koç University. He received numerous national scientific awards given to the outstanding young scientists. He has served as the Secretary General of Federation of Asian Chemical Societies (FACS). His research interests are nanomaterials, nanocatalysis, photocatalysis, hydrogen storage and sustainable organic transformations.

Melek Sermin Özer
Melek Sermin obtained her Ph.D. from Universität zu Köln in Organic Chemistry under the supervision of Prof. Albrecht Berkessel. She is currently working as a postdoctoral researcher in Metin Research Group and her research interests are photoredox organic transformations, carbon-based semiconducting materials, particularly carbon-based quantum dots.

Zafer Eroğlu
Zafer Eroğlu received his B.Sc. in Chemistry Education, M.Sc. and then his Ph.D. in Nanoscience and Nanoengineering from Atatürk University. He holds a position as a postdoctoral researcher in Metin Research Group at Koç University. His research interests are quantum dots, 2D nanomaterials, band engineering, photocatalysis, energy storage, removal of pollutants from wastewater and nanoparticles.

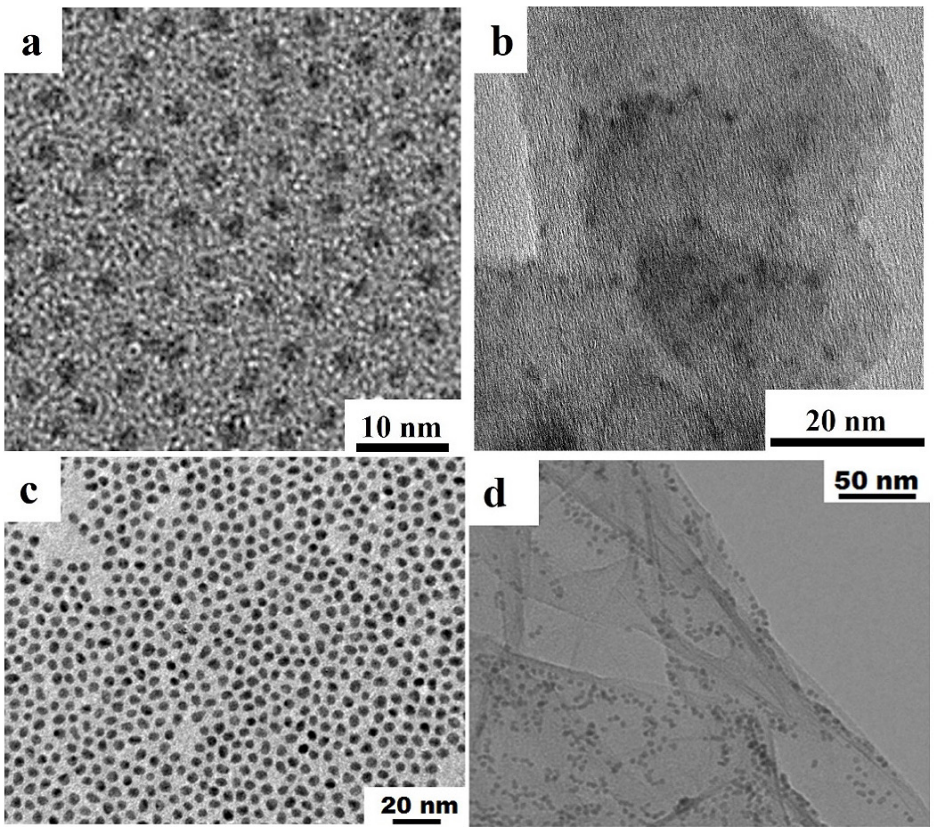

Figure 1. TEM images of (a) the colloidal 3.2 nm Ni NPs[16], (b) Ni/KC nanocatalyts. Reprinted (adapted) with permission from [16]. Copyright 2010 American Chemical Society. (c) the colloidal 4.5 nm Pd NPs[20] (d) Pd/rGO nanocatalysts. Reprinted from [21], Copyright 2012, with permission from Elsevier.

their scarcity and high cost. In this context, the preparation of bimetallic NPs in the form of alloys or core/shell, consisting of a noble metal and a first-row transition metal, is an advantageous way to prepare more economical catalysts. This idea has directed us to prepare bimetallic MPd, MPt and MRu alloy nanoparticles as catalysts for various reactions. However, our aim was not only to prepare high-quality bimetallic alloy or core/shell NPs, but also to achieve composition control between the metals and study their composition-controlled catalysis. The first monodisperse alloy NPs synthesized in our group were monodisperse CoPd alloy NPs as catalysts for the dehydrogenation of AB.[22] CoPd alloy NPs were prepared through a high-temperature solvothermal synthesis protocol comprising the thermal decomposition and reduction of cobalt(II) acetylacetonate ($Co(acac)_2$) and palladium(II) bromide ($PdBr_2$) in the presence of OAm and trioctylphosphine (TOP). It should be noted that the use of both $PdBr_2$ and TOP was found to be essential for the formation of monodisperse CoPd alloy structure, which is different from what we have reported in the synthesis of Pd NPs[20] As-synthesized CoPd NPs were then supported on KC (CoPd/KC) to be tested as catalysts. **Figure 2a** and **2b** show representative TEM images of colloidal CoPd alloy NPs and CoPd/KC nanocatalysts. From the TEM images, it can be concluded that 8 nm monodisperse spherical CoPd NPs were yielded by the developed recipe, and they were successfully deposited on KC via a simple ULPSA method by preserving their initial size and morphology. More importantly, the composition of the CoPd alloy NPs was controlled by tuning the initial molar ratio of the Co and Pd salts. Starting with metal salts with different Co/Pd ratios, five different CoPd alloy compositions ($Co_{79}Pd_{21}$, $Co_{35}Pd_{65}$, $Co_{27}Pd_{73}$, $Co_{14}Pd_{86}$, and Co_5Pd_{95} NPs) were yielded, respectively. Among all tested Co/Pd compositions, the $Co_{35}Pd_{65}$/KC catalyst was the most active one in the AB hydrolysis with a TOF of 1362 mol H_2.(mol Co+Pd)$^{-1}$.h^{-1}, which was higher than our Pd/rGO nanocatalysts[20]. The higher activity of $Co_{35}Pd_{65}$/KC nanocatalysts with a lower Pd content than Pd/rGO is mainly attributed to the synergism between Co and Pd in the alloy structure and the presence of two distinct metal atoms with the optimum ratio on the surface of NPs ensuring the optimum catalysis between catalyst and substrate at the intermediary strength, namely the Sabatier principle.[31]

In the synthesis recipe of CoPd alloy NPs described above, TOP had to be used to yield monodisperse alloy NPs. However, TOP attaches strongly to the surface of NPs due to the strong interaction between the lone pairs on phosphorus atoms and the surface metal atoms, resulting in deactivation. Therefore, we initiated a project to develop a general non-TOP synthesis protocol for the synthesis of MPd (M: Co, Ni and Cu) alloy NPs. After 3 years of the CoPd alloy NPs synthesis, we could develop a facile non-TOP synthesis protocol for the synthesis of NiPd, CuPd and CoPd alloy NPs. In this general recipe, selected metal precursors ($M(acac)_2$ or M(II) acetates) dissolved in OAm are injected into the hot surfactant + reducing agent (OAm + borane-*tert*-butlamine (BTB) or morpholine borane (MB)) solution at 100 °C in a four-necked glass reactor under argon atmosphere. By using this general recipe, we could successfully synthesize monodisperse CoPd[23], NiPd[25], and CuPd[24] alloy NPs, of which representative TEM images are shown in **Figure 3**. As it

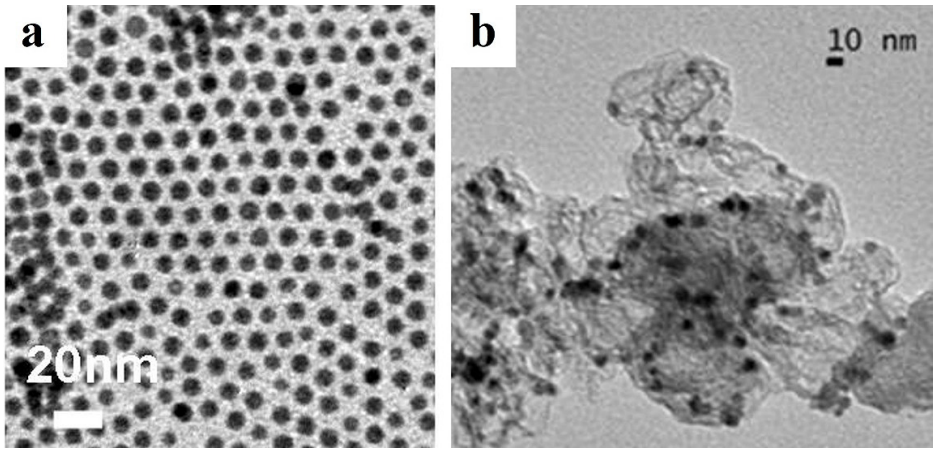

Figure 2. TEM images of (a) the colloidal 8 nm $Co_{35}Pd_{65}$ alloy NPs, (b) $Co_{35}Pd_{65}$/KC nanocatalyts. Reprinted (adapted) with permission from [23]. Copyright 2011 American Chemical Society.

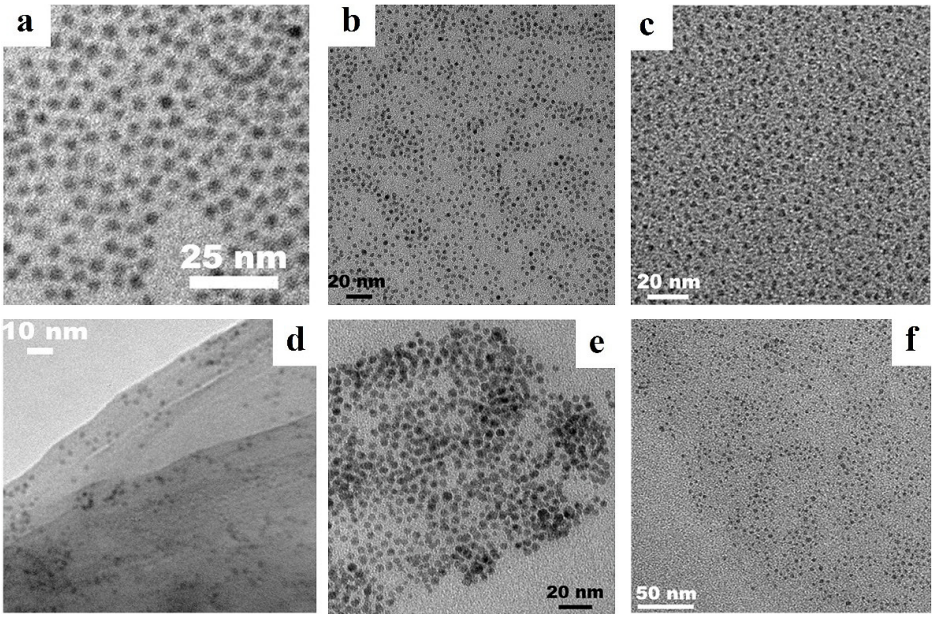

Figure 3. TEM images of (a) the 3.3 nm $Ni_{30}Pd_{70}$ alloy NPs Reprinted (adapted) with permission from [26]. Copyright 2014 American Chemical Society. (b) the 3.5 nm $Co_{30}Pd_{70}$ alloy NPs. Reprinted from [24], Copyright 2012, with permission from Elsevier. and (c) the 3.0 nm $Cu_{48}Pd_{52}$ alloy NPs, Reprinted (adapted) with permission from [25]. Copyright 2015 American Chemical Society. (d) $Ni_{30}Pd_{70}$/rGO nanocatalysts. Reprinted (adapted) with permission from [26]. Copyright 2014 American Chemical Society. (e) $Co_{30}Pd_{70}$/rGO nanocatalysts. Reprinted from [24], Copyright 2012, with permission from Elsevier. and (f) $Cu_{48}Pd_{52}$/rGO nanocatalysts. Reprinted (adapted) with permission from [25]. Copyright 2015 American Chemical Society.

can be concluded by the TEM images in **Figure 3a-c**, our recipe worked very well for the synthesis of monodisperse MPd (M: Co, Ni and Cu) alloy NPs with an average particle size of ca. 3 nm. Moreover, our developed recipe allowed us to synthesize MPd alloy NPs at different compositions by simply changing the ratio of precursors. use the yielded MPd alloy NPs as catalysts in the organic transformations, they were deposited on rGO via the ULPSA method. The NiPd/rGO (**Figure 3d**) and CoPd/rGO (**Figure 3e**) nanocatalysts were tested in the tandem dehydrogenation of AB and the transfer hydrogenation of nitroarenes.[23,25]

Both $Ni_{30}Pd_{70}$/rGO and $Co_{30}Pd_{70}$/rGO catalysts showed very high efficiency and selectivity for the conversion of a broad range of nitroarenes to anilines in a commercially available high-pressure glass thermolysis tube at room temperature (**Scheme 1**). Additionally, these nanocatalysts were stable and reusable for up to five consecutive runs. On the other hand, CuPd/rGO nanocatalysts were tested in the Sonogashira C–C cross–couplings.[24] A variety of aryl halides were successfully coupled to the biphenylacetylene derivatives with high to excellent yields via $Cu_{48}Pd_{52}$/rGO catalyzed Sonogashira cross-coupling reactions under mild/aerobic conditions.[22] Similar to NiPd or CoPd/rGO, $Cu_{48}Pd_{52}$/rGO nanocatalysts were also stable and reusable up to the five cycles without significant loss in their initial activity. In another study, we extended the application of $Cu_{48}Pd_{52}$/rGO nanocatalysts to tandem Suzuki-Miyaura and intramolecular C–H arylation reactions for the synthesis of substituted fluoranthenes.[26]

After our experience with the composition-controlled synthesis of MPd alloy NPs, we then extended our knowledge to develop one general recipe to synthesize MPt (M: Co, Ni, Cu) alloy NPs. In our recipe for the synthesis of monodisperse CuPt alloy NPs, platinum(II) and copper(II) acetylacetonates were co-reduced by BTB in a hot 1-octadecene (ODE) solution of OAm.[27]binary MPt (M = Co, Ni, Cu After the purification of the yielded MPt alloy NPs, they were supported on mesoporous graphitic carbon nitride (g-CN) to be used as electrocatalysts for the borohydride oxidation (BHOR) and hydrogen evolution reactions (HER). **Figure 4** shows the representative TEM images of MPt (M: Co, N, Cu) alloys and the MPt/g-CN nanocomposites. **Figure 4a-c** displays very-well dispersed monodisperse MPt alloy nanoparticles with the average particle size of 1.6 ± 0.3 nm for CoPt, 1.9 ± 0.4 nm for NiPt, 2.7 ± 0.5 nm for CuPt. Without any purification process, the yielded MPt alloy

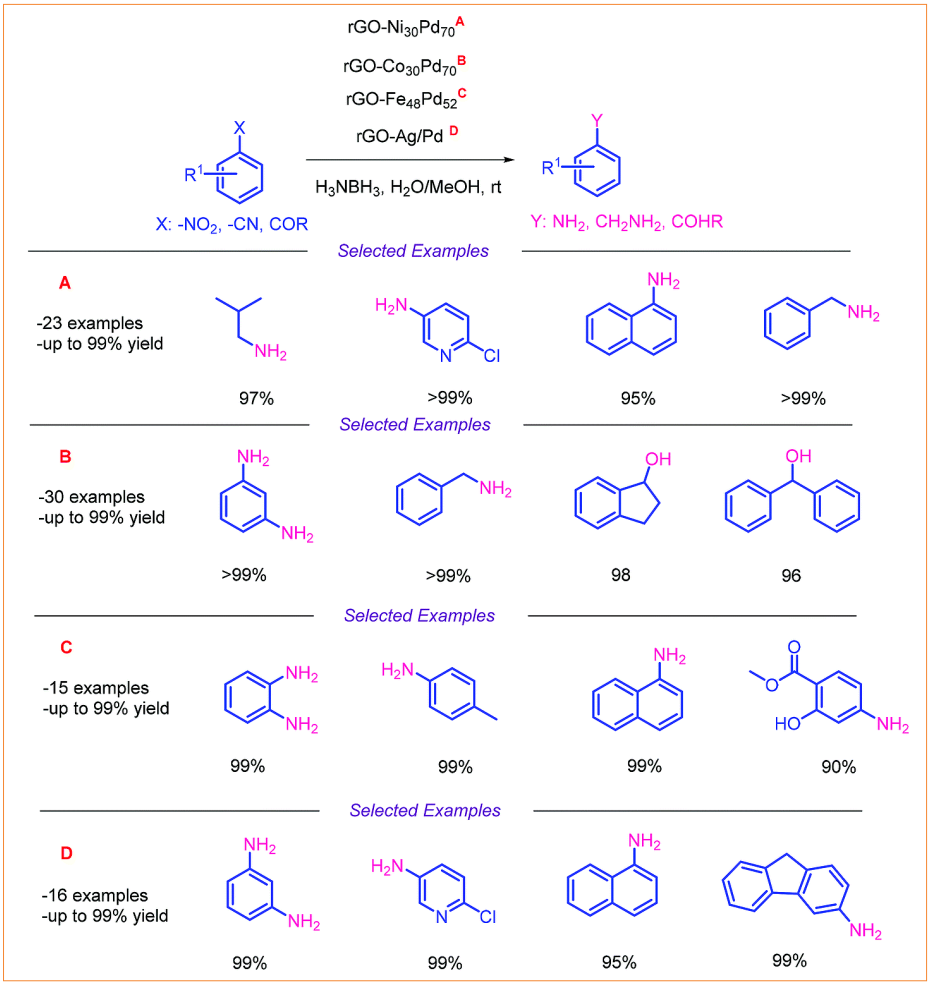

Scheme 1. rGO-supported bimetallic Pd NP-catalyzed transfer hydrogenation reactions. Reproduced from [33] with permission from the Royal Society of Chemistry.

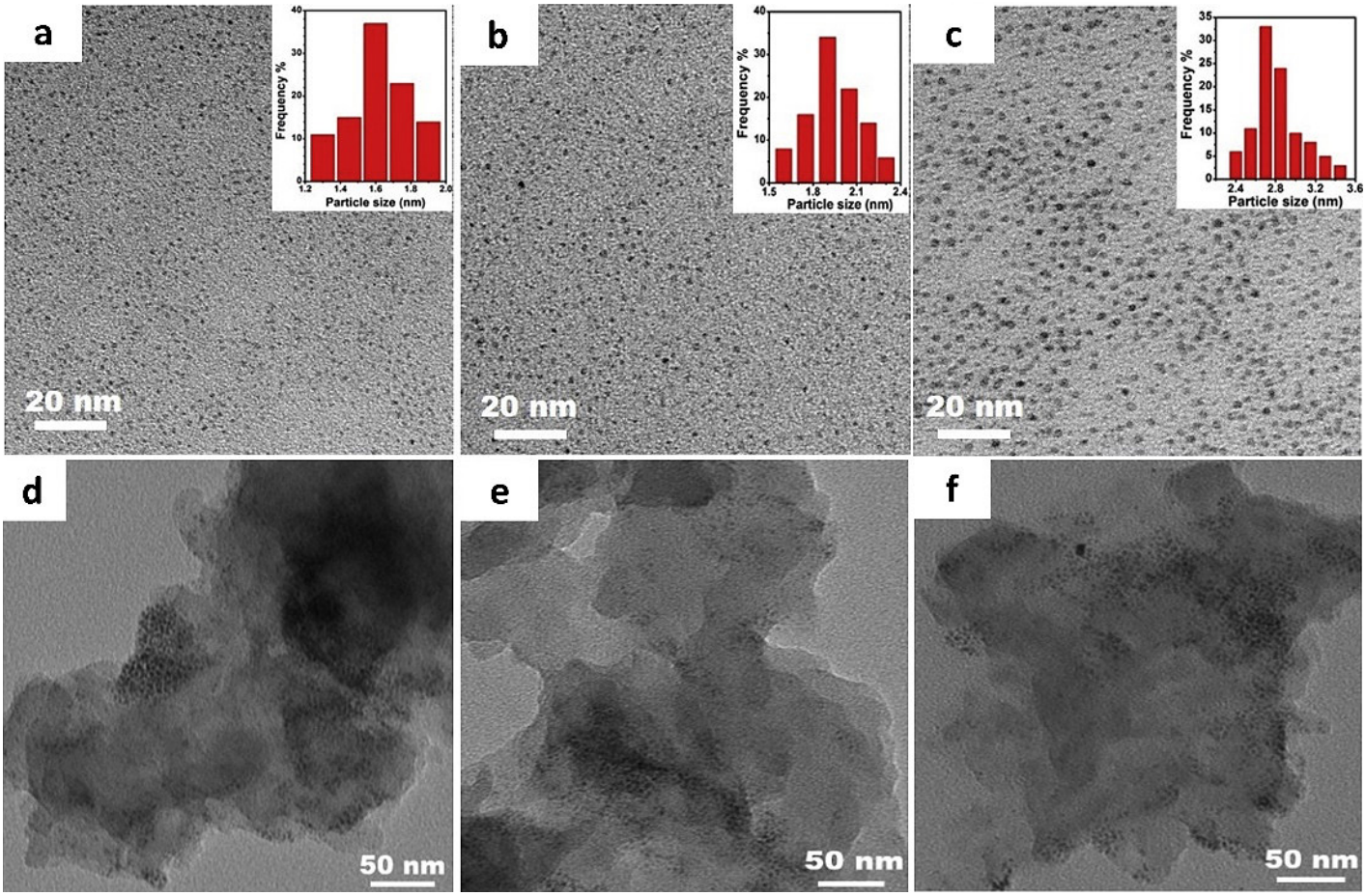

Figure 4. TEM images of (a) CoPt alloy NPs, (b) NiPt alloy NPs and (c) CuPt alloy NPs, (d) NiPt/g-CN nanocatalysts, (e) CoPt/g-CN nanocatalysts and (f) CuPt/g-CN nanocatalysts. Reprinted from [28], Copyright 2020, with permission from Elsevier.

NPs were assembled on g-CN via the ultrasound-assisted liquid phase self-assembly method. As shown by **Figure 4d-f**, all NPs were well-dispersed over g-CN nanosheets by preserving their initial size and morphology. However, it should be noted that there were some regional clumps observable for all MPt/g-CN nanocomposites, but those are not agglomerated particles, and they might be formed by the assembly of many MPt NPs in the same region. The Pt loading of MPt/g-CN nanocomposites was calculated to be 2.84 wt.% for CoPt, 2.33 wt.% for NiPt and 2.98 wt.% for CuPt through the ICP-MS analysis before their use as electrocatalysts for the BHOR and HER. Both HER and BOR current densities were observed to be, in general, higher for MPt nanoalloy electrocatalysts than in the case of Pt-based electrocatalysts. Among the MPt/g-CN electrocatalysts tested, CoPt/g-CN demonstrated the best performance for the HER while CuPt/g-CN provided the best BHOR activity.

After all these alloy NPs synthesis, we turned our attention to synthesizing several core/shell NPs. In the core/shell NP structure, one metal is found in the core and another metal forms a thin shell around the core. If core/shell NPs with non-precious metal core and thin, precious metal shell are rationally designed, very economical catalysts can be fabricated for various industrially important reactions. In this respect, we synthesized monodisperse Ni/Pd core/shell NPs for the Suzuki-Miyaura cross coupling[18] and the C–H arylation reactions.[19] Monodisperse Ni/Pd core/shell NPs were synthesis via one-pot protocol comprising the sequential thermal decomposition and the chemical reduction of the in-situ formed trioctylphosphine (TOP) complexes of Ni(II) and Pd(II) (Ni(II)-TOP and Pd(II)-TOP) from their commercially available precursors (Nickel(II) acetate and palladium(II) bromide). The key point in the recipe of Ni/Pd core/shell NPs is the in situ generation of Ni(II)-TOP and Pd(II)-TOP complexes which decompose and reduce at the temperature range of 190-210 °C and 230-245 °C, respectively. This sequential decomposition allowed the formation of Ni NPs as core and then the formation of thin Pd shell over the core NPs. **Figure 5** shows a representative TEM and STEM as well as the EDS elemental mapping images of Ni/Pd core/shell NPs. As easily concluded by the TEM image, very high quality, monodisperse 10 nm spherical NPs were produced (**Figure 5a**).[18] The STEM image (**Figure 5b**) and the associated EDS Ni and Pd mapping images (**Figure 5c**) revealed that Ni atoms were mainly in the core and Pd atoms are mainly on the shell, which is a clear indication of the Ni/Pd core/shell NPs formation. The as-prepared Ni/Pd core/shell NPs were then assembled on rGO to be employed as heterogeneous catalysts for the Suzuki-Miyaura C–C couplings of aryl halides and phenylboronic acid and then the C–H arylation of imidazo[1,2-a]pyridine with a variety of aryl halides.[19] **Figure 5d** shows a TEM image of as-prepared Ni/Pd-rGO catalyst. The Ni/Pd NPs were well-dispersed on few-layer rGO nanosheets by preserving their initial morphology and size. After the detailed structural characterization of the Ni/Pd-rGO nanocatalysts, they were first tested as catalysts in the Suzuki-Miyaura C–C coupling reactions. They were very active yet stable catalysts for the Suzuki–Miyaura cross-coupling of aryl boronic acids with aryl iodides, bromides, and even chlorides in a dimethylformamide/water mixture by

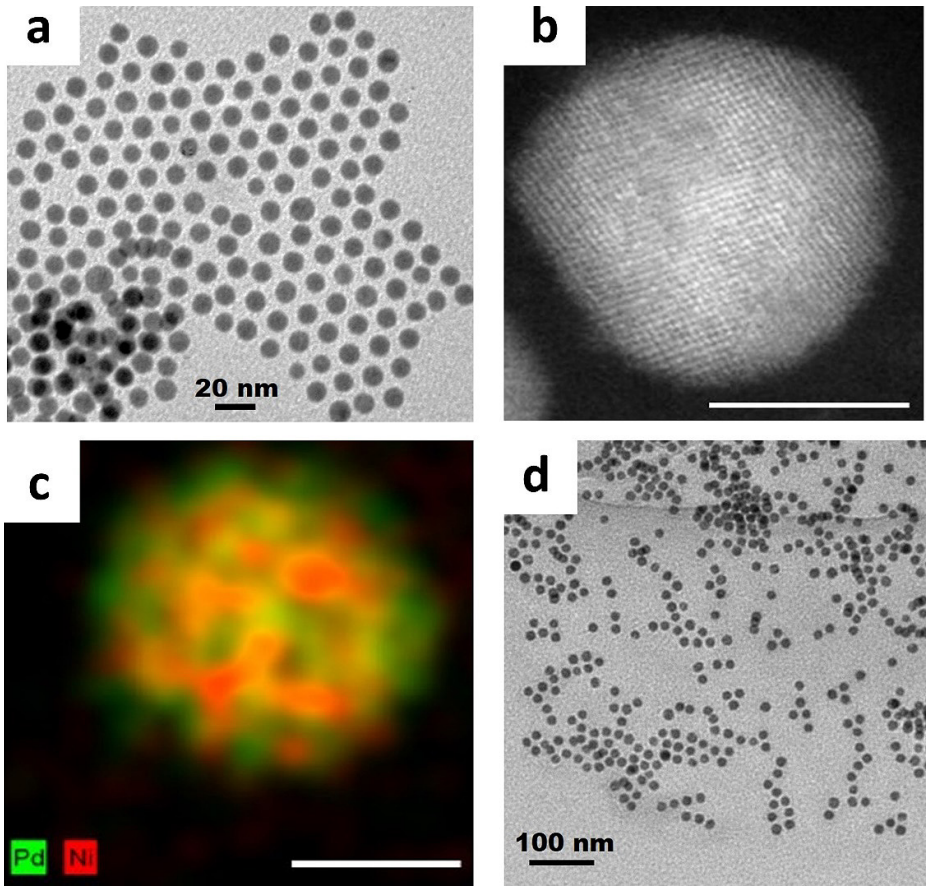

Figure 5. (a) TEM image of the Ni/Pd core/shell NPs, (b) STEM image of asingle Ni/Pd core/shell NPs (c) HAADF-STEM mapping image of a single Ni/Pd core/shell NPs, (d) Ni/Pd-rGO nanocatalysts. Reprinted (adapted) with permission from [19]. Copyright 2018 American Chemical Society

using K_2CO_3 as a base at 110 °C.[19] After almost five years later from this study, we extended to use of Ni/P/rGO as catalysts for the C–H arylation of imidazo[1,2-a]pyridine with a variety of aryl halides.[19] The Ni/Pd-rGO-nanocatalyst showed a wide substrate scope and functional group tolerance in the C–H bond arylation protocol.

All the above studies included the transition metal NPs, mostly noble metals, as catalysts, but as it is aforementioned, the use of these metals as catalysts is impractical in terms of sustainability. The ultimate target in sustainable chemistry is catalyzing the chemical reactions with the non-metallic catalysts, of course if it is possible thermodynamically. In this respect, we have changed our focus from purely metal-based transition metal nanocatalysts to non-metallic ones that utilize solar light for possible catalytic applications, which has allowed us to develop more sustainable chemical transformations. The following section summarizes our research group's recent studies on the rational design of non-metallic two-dimensional (2D) semiconductor-based photocatalysts for different chemical conversions.

Changing the energy source: Solar light

The imitation of nature's principles across various domains stands as a compelling impetus for scientists. Given the finite nature of energy resources on our planet and their escalating depletion in tandem with global population growth, harnessing solar light has emerged as a viable solution.[34] Photocatalysis, a transformative process within sustainable chemistry, presents a myriad of advantages in contrast to traditional catalysis. Diverging from conventional techniques, photocatalysis epitomizes a more environmentally conscious approach by functioning under gentle conditions and circumventing the necessity for harsh reagents. After the discovery of various carbon allotropes, a new type of carbon-based polymeric material called graphitic carbon nitride (g-CN) has emerged in scientific literature.[35] This material has been utilized for two main purposes: as a support material for the deposition of nanoparticles and as a non-metallic semiconductor photocatalyst. Its appeal lies in its easy synthesis, consisting of earth-abundant elements (C, N and H), high stability and versatility, which makes it a suitable photocatalysts for a broad range of applications. One particular application involves its use as a support material to enhance the catalytic activity of the metal NPs for hydrolysis of AB.[36] To enhance the efficiency of this process, we turned to g-CN as a support material for the AgPd alloy NPs and photosensitizer. We assembled monodisperse AgPd alloy NPs onto 2D g-CN nanosheets to create a composite material. This composite has dual benefits: *i*) the presence of g-CN helps to stabilize the colloidal NPs since colloidal NPs can sometimes be kinetically unstable, leading to aggregation or other undesirable effects. By decorating the NPs on the g-CN support, they become more stable and better suited for catalytic purposes, *ii)* photocatalytic activity in the visible light region: the g-CN support has a suitable bandgap of 2.7 eV, which means it can efficiently absorb visible light. In order to compare the superiority of g-CN, graphene oxide and Ketjen Black were also used to assemble AgPd NPs. Among them, the catalysts composed of g-CN@$Ag_{42}Pd_{58}$ exhibited the highest level of activity compared to other catalyst components. This enhanced activity was attributed to the Schottky junction formation, which was driven by the efficient charge separation arising from the photogenerated electron flow between g-CN and metal NPs present in the catalyst **Figure 6a**. Furthermore, the activity of the g-CN@$Ag_{42}Pd_{58}$ catalyst was additionally improved through treatment with acetic acid (AAt), leading to a remarkable initial turnover frequency of 94.1 mol H_2·(mol catalyst)$^{-1}$·min^{-1}. Additionally, the g-CN@$Ag_{42}Pd_{58}$-AAt catalyst demonstrated good stability during the hydrolysis of AB.

To further enhance the photogenerated charge carriers, visible light harvesting ability, and absorption capacity of g-CN, we have used the strategy of creating heterojunctions. The remarkable stability of g-CN, combined with the wide-range absorption capability of black phosphorus (BP) and its unique features, makes them an ideal pair for the construction of a heterojunction system. Therefore, we developed a photocatalyst based on this concept, where we explore the influence of ratios for both AgPd alloy NPs and g-CN/BP. This photocatalyst is denoted as g-CN/BP-AgPd and is used as a photocatalyst in the methanolysis of AB. The optimal catalytic performance of g-CN/BP-AgPd nanocomposites was achieved when using a 5/1 (wt/wt) ratio of g-CN to BP and employing an $Ag_{50}Pd_{50}$ alloy composition under blue LED illumination at room temperature. Moreover, treating the ternary nanocomposites with acetic acid resulted in further enhancement of their activity, with a reported high initial turnover frequency of 43.7 mol H_2·(mol catalyst)$^{-1}$·min^{-1}. The underlying reason behind this superior

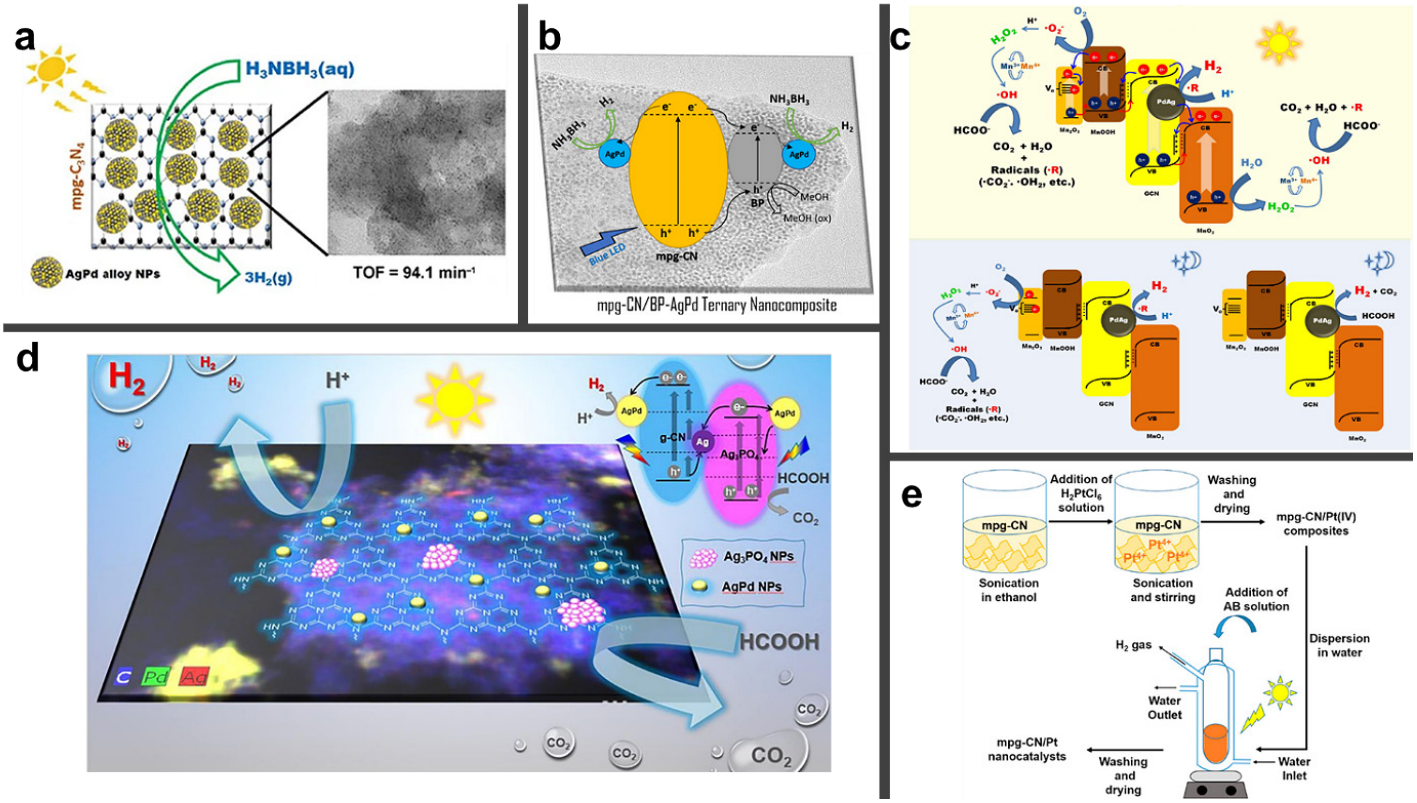

Figure 6. The proposed formation of Schottky junction between (a) g-CN and metal NPs. Reproduced with permission from 36. Copyright 2016 Springer Nature. (b) g-CN/BP and metal NPs. Reprinted (adapted) with permission from [20]. Copyright 2020 American Chemical Society. (c) A plausible reaction mechanism of g-CN/MnO_2/MnOOH for FA dehydrogenation under light and dark, respectively, Reprinted from [39], Copyright 2022, with permission from Elsevier. (d) The proposed mechanism of g-CN/Ag/Ag_3PO_4-AgPd for FA dehydrogenation under visible light illumination, Reprinted from [40], Copyright 2021, with permission from Elsevier. (e) The synthesis of gCN/a-WO_x/Pt nanocatalysts for AB hydrolysis. Reprinted (adapted) with permission from [37]. Copyright 2020 American Chemical Society.

photocatalytic activity was explained by the flow of photogenerated electrons from g-CN/BP heterojunction to the surface of alloy NPs shown in **Figure 6b**.

Further investigations involve the *in situ* synthesis of Pt NPs supported on g-CN nanosheets during the hydrolytic dehydrogenation of AB.[37] The catalytic activity of the resultant g-CN/Pt nanocatalysts is evaluated for hydrogen generation from AB hydrolysis under white light illumination. Pt NPs are shown to exhibit size and shape-dependent activity in AB hydrolysis, leading to a detailed examination of Pt loading effects on particle size and catalytic activity. The *in-situ* synthesis protocol demonstrates the unique role of g-CN, acting as both a support material and stabilizer for Pt NPs. The as-prepared g-CN/Pt nanocatalysts exhibit excellent photocatalytic activity in AB hydrolysis under white-light irradiation at room temperature (**Figure 6e**). Remarkably, the g-CN/Pt nanocatalysts prove to be robust and reusable catalysts, making them promising candidates for photocatalytic hydrogen generation systems employing AB as a solid hydrogen storage material. Later, we were motivated to develop the performance of g-CN/Pt to construct a Z-scheme with WO_3.[38] which is higher than that of gCN/Pt nanocatalysts (287.7 mol H_2 mol Pt^{-1} min^{-1} The Z-scheme of g-CN and WO_3 is a highly efficient electron transfer mechanism, where photoexcited electrons from g-CN reduce WO_3, leading to enhanced photocatalytic activity in many transformation reactions. This study aimed to synthesize g-CN/WO_3 heterojunctions and explore their potential as visible light active support material for the *in situ* synthesis of Pt NPs and concurrent hydrogen generation from AB under visible light irradiation. To achieve this goal, a novel one-pot synthesis protocol was employed, involving the thermal polymerization of urea in the presence of tungstate salts to fabricate g-CN/WO_3 support materials. However, the obtained results directed the research towards investigating g-CN/a-WO_x heterojunctions, encompassing amorphous oxygen-deficient/nonstoichiometric tungsten oxide (a-WO_x) species with continuously modified electronic structure and optical properties, dependent on the valence state of W. Subsequently, Pt NPs were grown on the as-prepared gCN/a-WO_x nanocomposites during hydrolysis of AB. The study further explored the impact of white light and W content on the photocatalytic activity of gCN/a-WO_x/Pt nanocatalysts. The gCN/a-WOx/Pt nanocatalyst loaded with 4.72 wt% W and 0.679 wt% Pt achieved the highest turnover frequency value of 419.2 $mol_{(hydrogen)}$·$mol_{(catalyst)}^{-1}$·min^{-1}. This TOF value was remarkably higher than that of gCN/Pt (287.7 $mol_{(hydrogen)}$·$mol_{(catalyst)}^{-1}$·min^{-1}).

Formic acid (FA) was also studied because of distinguishes itself as an exceptional hydrogen carrier due to its non-toxic, non-flammable, and stable nature. Furthermore, it is a readily available and cost-effective liquid organic molecule that remains stable under ambient conditions, making it stand out among various other potential hydrogen carriers.[39] Our group has aimed to develop more effective photocatalysts for FA dehydrogenation by designing a Z-scheme heterojunction that utilizes a higher hole potential than pristine g-CN.[40] A novel Z-scheme photocatalyst, denoted as g-CN/Ag/Ag_3PO_4-AgPd was fabricated, where Ag_3PO_4 was chosen as the second semiconductor due to its beneficial properties, including narrow bandgap and strong oxidizing ability. The Z-scheme heterojunction photocatalyst exhibited exceptional catalytic

activity in FA dehydrogenation, with a turnover frequency value of 2107 mol H_2·(mol catalyst)$^{-1}$·min^{-1}, which was significantly higher than other photocatalysts, including g-CN/Pd and g-CN/AgPd. Mechanistic investigations confirmed the effectiveness of holes in the photocatalytic reaction, and the reusability tests revealed the importance of Ag_3PO_4 in the catalytic activity (**Figure 6d**). Further exploration if a g-CN-based S-scheme heterojunction, formed with a semiconductor possessing a higher VB potential than Ag_3PO_4 used in our previous work, could lead to enhanced photocatalytic activity in FA dehydrogenation. Accordingly, a novel S-scheme heterojunction between g-CN and MnO_2 was synthesized, given its more positive VB potential than Ag_3PO_4.[39] However, through the incorporation of a hydrothermal treatment process into the literature method, we discovered that a ternary nanocomposite, g-CN/MnO_2/MnOOH, and it demonstrated a remarkable photocatalytic FA dehydrogenation (turnover frequency value of 3919 mol H_2·(mol catalyst)$^{-1}$·min^{-1}) upon the addition of PdAg NPs into the structure. Detailed characterization of g-CN/MnO_2/MnOOH revealed the presence of 2D δ-MnO_2 nanosheets and 1D γ-MnOOH nanorods, along with thin Mn_2O_3 layers on the nanorod surface, as well as ultra-small PdAg NPs decorating g-CN nanosheets through the reduction of metal salts with $NaBH_4$ aqueous solution. Remarkably, the photocatalytic FA dehydrogenation activity of g-CN/MnO_2/MnOOH-PdAg was ascribed to scavenger experiments and the presence of manganese oxide species in the photocatalyst facilitated the decomposition of H_2O_2, formed during the photocatalytic process, into •OH radicals, which exhibited high reactivity in the oxidation of $HCOO^-$ to CO_2 in the dehydrogenation mechanism (**Figure 6c**). Notably, this conclusion had not been addressed in any report on photocatalytic FA dehydrogenation, although it is highly likely to be observed to some extent in various semiconductor photocatalysts used in this application thus far. Additionally, radical trapping tests surprisingly revealed that the presented heterojunction photocatalysts exhibited FA dehydrogenation activity even in the dark, particularly at ambient temperatures. This phenomenon was attributed to the storage of electrons in the Mn_2O_3 layer formed over 1D γ-MnOOH nanorods, possibly due to oxygen vacancies, leading to the formation of defect sites in the band structure of the Mn_2O_3 layers.

In the photocatalytic HER process, a photocatalyst material is used to facilitate the splitting of water molecules into hydrogen and oxygen using sunlight or other sources of light. This process also is of significant interest in the field of renewable energy and sustainable technologies because hydrogen gas is considered a clean and versatile fuel source that can be used for various applications, including electricity generation and as a clean fuel for vehicles. The ultimate goal is to develop cost-effective and environmentally friendly methods for producing hydrogen gas using renewable energy sources like sunlight, which could contribute to a more sustainable energy future.[42] A new ternary nanocomposite, referred to as mpg-CN/BP-Au, was created and thoroughly characterized for its potential in two distinct applications: photocatalytic hydrogen evolution driven by visible light and electrochemical sensing.[43] The nanocomposite exhibited impressive performance in both areas. When subjected to 8 hours of visible light exposure, the mpg-CN/BP-Au nanocomposite demonstrated a hydrogen generation rate of up to 1024 μmol g^{-1}, which was double that of the original mpg-CN material (559 μmol g^{-1}). A comprehensive assessment of existing research was undertaken to compare the obtained outcomes. In the context of electrochemical sensing, the mpg-CN/BP-Au/GCE (graphite carbon

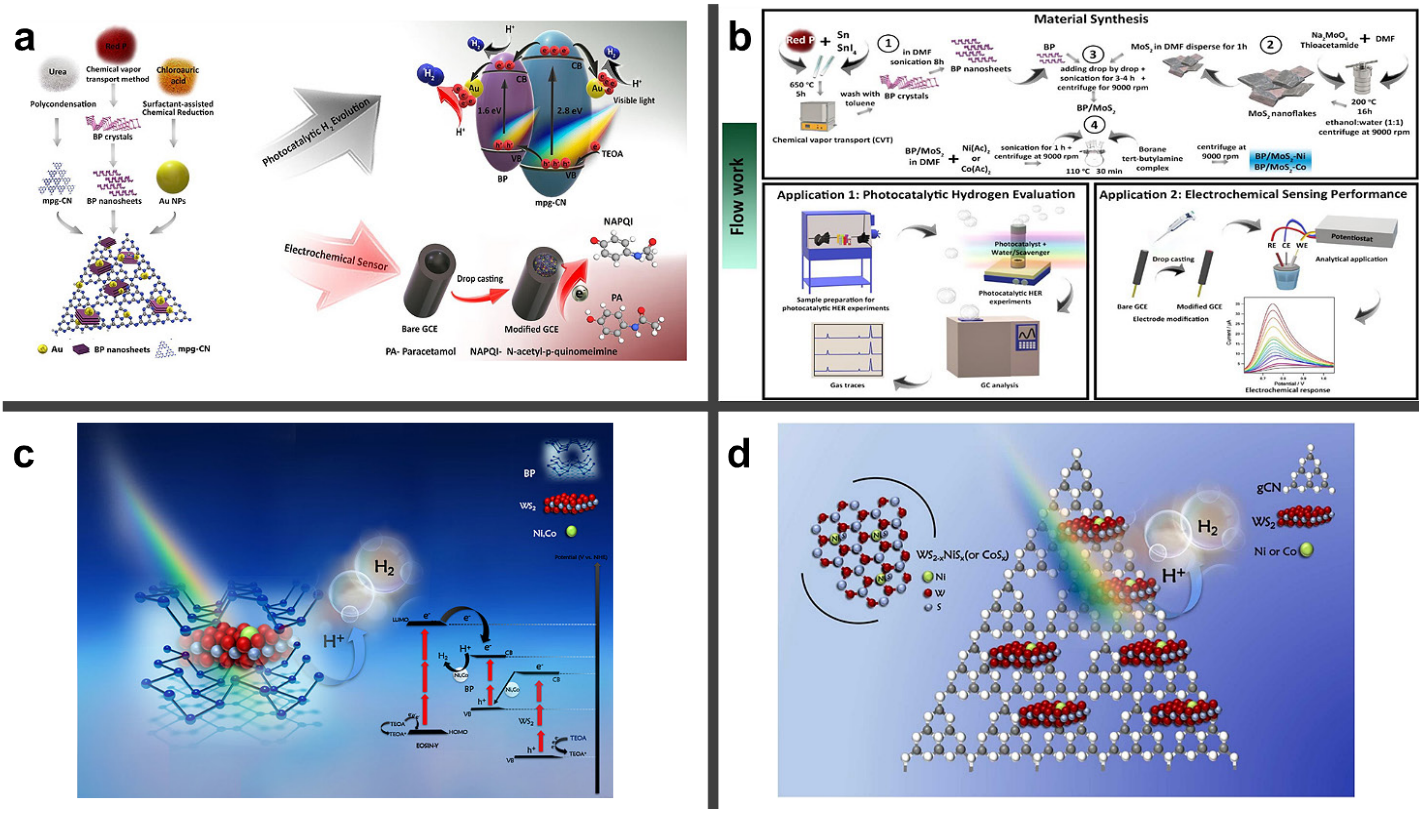

Figure 7. (a) The synthesis of gCN/BP/Au and the proposed mechanism for HER and electrochemical sensing. Reprinted from [42], Copyright 2021, with permission from Elsevier. (b) The synthesis of BP/MoS_2-M (M: Ni, Co) for HER and electrochemical sensing. Reprinted from [43], Copyright 2023, with permission from Elsevier. The proposed mechanism of (c) BP/WS_2-M (M: Ni, Co), (d) gCN/WS_2-M (M: Ni, Co) Reprinted from [45]. Copyright 2023, with permission from Elsevier for HER under visible light illumination.

electrode) assembly displayed a linear detection range for paracetamol spanning from 0.3 to 120 µM, with a minimum detectable concentration of 0.0425 µM under optimal conditions. The enhanced catalytic and photocatalytic activity of the mpg-CN/BP-Au nanocomposite can be attributed to the formation of heterojunctions between BP and g-CN materials. This heterojunction structure resulted in improved absorption of visible light and reduced recombination of photocarriers. Moreover, the presence of Au nanoparticles contributed to an accelerated adsorption rate of mpg-CN/BP-Au due to their exceptional electrical properties and spillover effect. The porous architecture of mpg-CN/BP-Au facilitated efficient charge carrier movement for both photocatalytic hydrogen production and electrochemical sensing (**Figure 7a**).

We continued to develop innovative heterojunction photocatalysts by creating transition metal NPs anchored on pre-prepared gCN/BP binary heterojunctions, termed gCN/BP-M (M: Co, Ni, and Cu).[44] These novel heterojunctions were utilized as visible-light driven photocatalysts for the photocatalytic HER. Characterization of the binary and ternary nanocomposites revealed the establishment of type I heterojunction between g-CN and BP, with additional Schottky junctions formed between metal NPs and g-CN/BP nanocomposites upon the generation of transition metal NPs. The g-CN/BP-M nanocomposites exhibited enhanced optical properties and charge kinetics compared to g-CN and gCN/BP, leading to improved catalytic activity in the photocatalytic HER under visible light illumination. Remarkably, the g-CN/BP nanocomposites produced 3.6 times more H_2 gas than pristine g-CN nanosheets, and this activity was further enhanced with the introduction of Ni, Co, and Cu NPs on them. The g-CN/BP-Ni ternary nanocomposites demonstrated the highest photocatalytic H_2 evolution activity among all materials tested, achieving 4.7-fold and 1.3-fold higher activity compared to pristine g-CN and g-CN/BP binary heterojunctions, respectively. In addition to experimental findings, a density functional theory (DFT) study showed that ternary nanocomposites were primarily composed of g-CN over BP, and the inclusion of Ni NPs led to a narrowed band gap and improved visible light absorption of the g-CN/BP binary heterojunctions. This enhancement in photocatalytic activity was attributed to increased photon absorption and improved charge separation on the 2D/2D heterojunction. The g-CN/BP-Ni nanocomposites displayed remarkable stability under visible light irradiation for an extended period, producing 2.63 mmol g^{-1} H_2 in 8 hours, which was significantly higher than that produced by pristine m-gCN (0.559 mmol g^{-1} H_2) and g-CN/BP binary heterojunctions (2.03 mmol g^{-1} H_2). The study conclusively demonstrated that the photocatalytic activity of g-CN/BP binary heterostructures for HER can be further enhanced by depositing transition metal NPs on them, particularly Ni NPs.

In the next study, we developed a straightforward approach to enhance the photocatalytic activity of binary g-CN/MoS_2 heterojunctions by doping them with Ni or Co via a chemical reduction method.[45] By depositing MoS_2 onto g-CN through an in-situ solvothermal method, a "type-I" heterojunction was formed. The subsequent doping with Ni and Co further improved the photocatalytic HER under visible light illumination, thanks to the creation of S-deficient MoS_{2-x} nanostructures when exposed to light. Notably, this novel strategy achieved Ni or Co-doped g-CN/MoS_2 heterojunctions with very low metal loading (0.1 wt%), resulting in a heterojunction with S-deficiency MoS_2 structures. As a result, the g-CN/MoS_2-Ni and g-CN/MoS_2-Co heterojunctions exhibited significantly higher

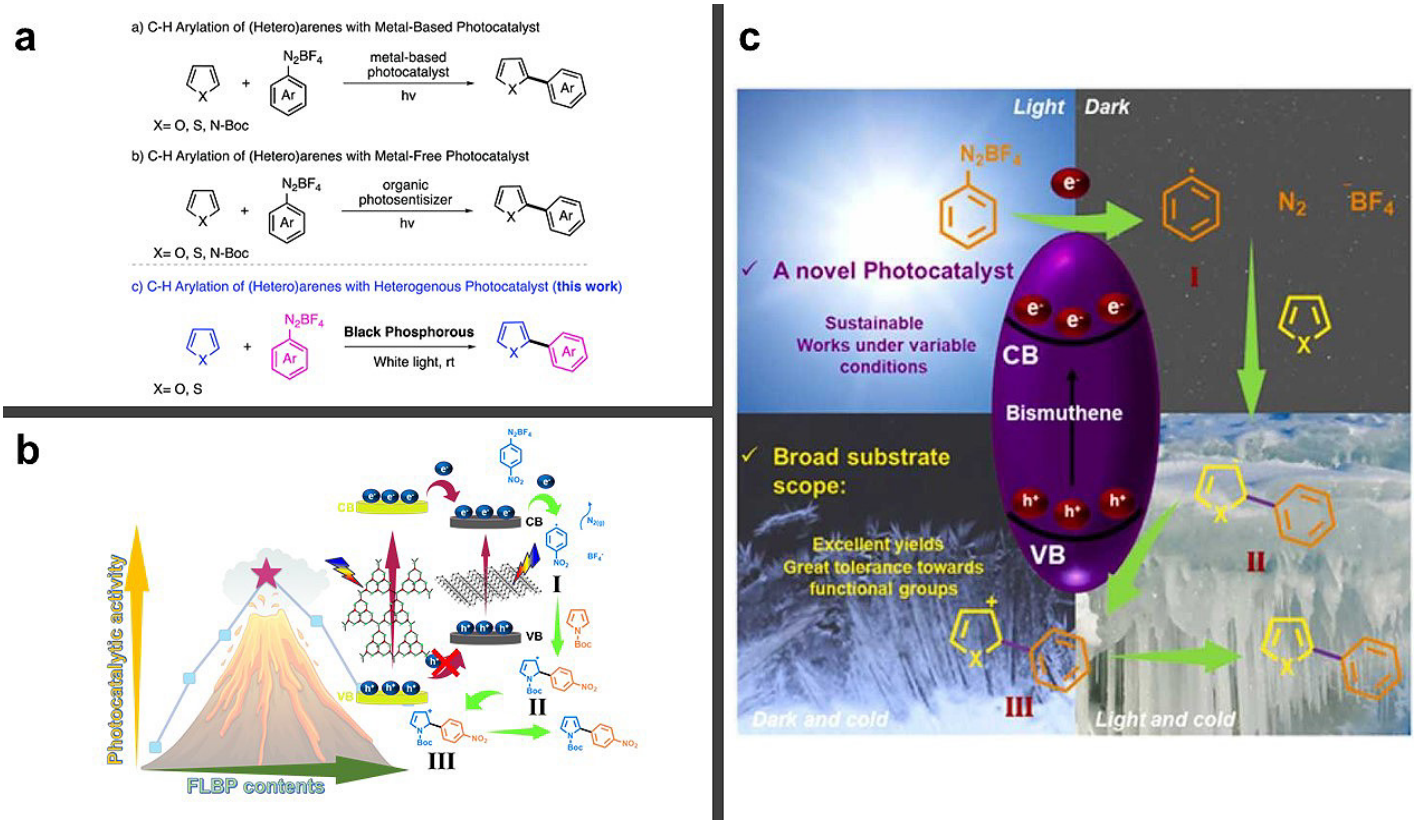

Figure 8. (a) C-H arylation reactions via traditional methods vs. our strategy. Reproduced from[50] with permission from the Royal Society of Chemistry., Plausible reaction mechanism of (b) FLBP/gCN. Reproduced from [51] with permission from the Royal Society of Chemistry., (c) Bismuthene for C–H arylation reactions. Reprinted from [52], Copyright 2022, with permission from Elsevier.

photocatalytic H_2 evolution performance compared to g-CN/MoS_2 heterojunctions by enhancing the separation rate of photogenerated electron-hole pairs. The HER activity for g-CN/MoS_2-Ni and g-CN/MoS_2-Co samples reached 5.924 and 5.159 mmol g^{-1}, respectively, in 8 hours. The increased hydrogen generation with Ni or Co-doped g-CN/MoS_2 heterojunctions can be attributed to effective electron-hole separation and the creation of MoS_{2-x} nanostructures, providing more active sites for H_2 generation. We also proposed an electron migration mechanism based on the band-edge potentials of g-CN and MoS_2 to explain the enhanced photocatalytic activity of g-CN/MoS_2-Ni, Co heterojunctions

In another study, novel BP/MoS_x, BP/Cu, and BP/Pt nanocomposites were successfully synthesized at liquid/liquid interfaces.[46] The catalysts were thoroughly characterized using advanced analytical techniques. The catalytic activity of MoS_x was compared to Pt and Cu nanoparticles, given their similar redox potentials. MoS_x nanostructures exhibited better dispersion on BP nanosheets compared to metallic nanoparticles, resulting in higher durability in the catalytic HER. The BP-based nanocomposites displayed superior catalytic activities compared to their pristine forms, attributed to enhanced electron transport through synergistic effects and heterojunction formation between BP and metal nanoparticles. Additionally, the nanocomposites had increased active sites due to more homogeneous particle distribution and reduced agglomeration. Among the BP-based nanocomposites, BP/MoS_x displayed the highest catalytic activity, likely because anchoring MoS_x onto BP nanosheets preserved the oxidation of both catalyst particles and BP nanosheets. Kinetic calculations revealed that BP/MoS_x nanocomposites were the most efficient HER catalysts, significantly increasing reaction rates compared to the absence of a catalyst or the presence of free MoS_x. BP-based nanocomposites exhibited efficient catalytic activities for HER due to their enhanced conductivity properties, active sites, and surface area.

In comparison to the previous study, in this work, we focused on using 2D semiconductor-based Ni or Co doped black phosphorus/molybdenum disulfide (BP/MoS_2–Y (Y: Ni, Co)) heterojunctions for dual applications in photocatalytic hydrogen evolution and as a novel electrochemical nitrite sensor (**Figure 7b**).[47] The fabricated BP/MoS_2–Y (Y: Ni, Co) heterojunctions demonstrated significantly enhanced photocatalytic hydrogen evolution activity under visible light illumination, utilizing Eosin Y (EY) sensitizer and triethanol amine (TEOA) electron donor. The H_2 generation rate of BP/MoS_2–Ni and BP/MoS_2–Co nanostructures reached 65.202 mmol g^{-1} and 68.455 mmol g^{-1}, respectively, within 8 hours of photocatalytic reaction, which were approximately 1.58 and 1.66 times higher than unsupported BP/MoS_2 heterojunctions. The improved hydrogen evolution was attributed to the formation of a heterojunction between BP and MoS_2, and the presence of Ni or Co as cocatalysts facilitated the easy reduction of protons for H_2 generation.

In another study, 2D/2D binary heterojunctions of BP and tungsten disulfide (WS_2) was successfully prepared and investigated their photocatalytic activity for HER under visible light irradiation.[48] The pristine BP showed weak photocatalytic activity due to fast recombination of photoinduced charge carriers. However, the BP/WS_2 heterojunction catalyst exhibited approximately three times higher hydrogen production with a solar-to-hydrogen (STH) efficiency of 5.7%, attributed to the large contact areas facilitating photogenerated charge transfer. Incorporating earth-abundant transition metal (Ni or Co) NPs further enhanced the HER activity of the BP/WS_2 binary nanocomposites. The presence of Co NPs as a co-catalyst in BP/WS_2 binary heterojunction significantly improved the STH efficiency to 31.2%, attributed to increased photon absorption, active sites, and longer charge carrier lifetime through reduced recombination rates. The ternary heterojunction catalysts, BP/WS_2-Ni and BP/WS_2-Co, showed 3.2 times and 2.9 times more hydrogen evolution, respectively, compared to BP/WS_2. This noble-metal-free catalyst system demonstrated high stability and efficiency in photocatalytic hydrogen production. The study suggests that BP/WS_2 binary heterojunctions offer specific active sites and higher photocatalytic efficiency than pristine BP nanosheets under visible light (**Figure 7c**). We replaced BP with g-CN and the preparation of ternary g-CN/WS_2-Y (Y: Ni, Co) heterojunctions using the chemical reduction method for the photocatalytic HER was studied.[49] The pristine WS_2 semiconductor was grown on 2D g-CN material through the hydrothermal method. The heterojunction structure, morphology, and photophysical properties were extensively characterized. The g-CN/WS_2-Ni and g-CN/WS_2-Co heterojunctions were designed to enhance the photocatalytic hydrogen evolution activities compared to g-CN/WS_2. Under visible light irradiation, the HER activities of g-CN/WS_2-Ni and g-CN/WS_2-Co were about 2-fold and 1.5-fold higher, respectively, than that of g-CN/WS_2. Moreover, their STH efficiencies were calculated as 0.61%, 0.64%, 0.56%, and 0.32% for g-CN/WS_2-Ni, g-CN/WS_2-Co, g-CN/WS_2, and g-CN, respectively. The 2D/2D heterojunction between gCN and WS_2 facilitated effective electron transfer and enhanced light harvesting compared to pristine gCN or WS_2. The transition metal-doped heterojunctions exhibited increased activity and stability due to reduced recombination rate and prolonged charge carriers' lifetime in the formed S-scheme heterojunction (**Figure 7d**). The improved photocatalytic activity was attributed to the interaction between transition metals and S^{-2}, resulting in defects due to sulfur atom deficiency in WS_2, and efficient charge migration in the formed S-scheme heterojunction. The presented ternary heterojunction holds promise for significant contributions to the field of photocatalysis and potential applications in photoredox catalysis due to its favorable properties.

The arylation of heteroarenes holds significant importance in organic chemistry as it enables the synthesis of molecular structures that form crucial frameworks in functional materials with desirable optical and electronic properties and biological activity.[50–53] While traditional cross-coupling reactions have been widely used for this purpose, the need for pre-activation of heteroarenes and functionalized coupling partners limits their applicability.[54] Consequently, the direct C–H activation strategy for heteroarene arylation has gained attention in recent years. The conventional approach involves precious metal catalysts like Pd and Ru at high temperatures, but visible-light-mediated photocatalytic methods have emerged as a promising alternative.[51] However, these photo-induced C–H activations mostly rely on costly and toxic noble-metal complexes, prompting the exploration of metal-free photocatalysts such as EY. Despite their potential, the practical application of organic chromophores like EY requires special chromatographic purification methods due to their solubility in most organic solvents.[53] Therefore, we present a groundbreaking approach by utilizing BP as a metal-free, visible-light-responsive, and reusable heterogeneous photoredox catalyst for the direct C–H arylation of furan and thiophene derivatives with aryl diazonium salts under visible-light irradiation at room temperature (**Figure 8a**).[55] This marks the first instance of employing BP as an efficient and environmentally friendly catalyst for such transformations, further advancing the field of visible-light-mediated C–H functionalization. However, we got motivated to develop BP catalyzed C–H functionalization method further since BP limits reusability procedure owing to its low chemical stability. In the pursuit of designing efficient photocatalysts with favorable optical, chemical/thermal properties, and long-term stability, the combination of 2D materials composed of earth-abundant

elements to form heterojunctions emerges as an environmentally friendly option. In this research, a remarkably effective photoredox catalyst was developed by creating a binary heterojunction using few-layer BP (FLBP) and g-CN.[56] This synergistic FLBP/g-CN heterojunction demonstrated exceptional activity in the photoredox C–H arylation of heteroarenes with diazonium salts under visible light irradiation, leading to product yields of up to 94% under ambient conditions (**Figure 8b**). Interestingly, the FLBP/g-CN activity exhibited a volcano-shaped relationship concerning the BP loading ratios, with the best performance achieved at 35 wt% FLBP. A comprehensive investigation of the substrate scope was conducted to comprehend its restrictions concerning various heteroarenes (furan, thiophene, and *N*-Boc pyrrole) in conjunction with diazonium salts containing both electron-donating (ED) and electron-withdrawing (EWD) groups, encompassing a total of 29 examples. Moreover, the mechanistic studies and charge migration experiments allowed the proposition of a unique band diagram illustrating distinct electron-hole migration between g-CN and FLBP, deviating from nonclassical type-I heterojunction in the heterojunction structure.

After sparkling of BP, researchers have been exploring the potential of 2D semiconductor materials composed of group 15 elements (pnictogens) as efficient photocatalysts in various applications. However, there has been no example of using bismuthene as a photocatalyst until our report, for the first time, the use of bismuthene as a highly efficient photocatalyst in a liquid-phase organic transformation. Bismuthene exhibits its remarkable photocatalytic properties under various reaction conditions.[57] The photoredox C–H arylation of (hetero)arenes, achieving high product yields of up to 98% under indoor light illumination, darkness, outdoors, and low temperatures (**Figure 8c**). This protocol worked efficiently on a wide range of substrates, not only heteroarenes (furan, thiophene, and pyrrole) and but also arenes (benzene and nitrobenzene) with aryl diazonium salts (total of 43 examples) possessing both electron-withdrawing and electron-donating groups. To gain insights into the catalytic activity of bismuthene, DFT calculations were performed and indicated a possible electron transfer towards arenes increasing their reactivity. The study revealed the underlying mechanistic details that contribute to the remarkable catalytic performance of bismuthene in the C–H arylation of (hetero)arenes.

The unique versatility of g-CN is its skeleton consisting of carbon and nitrogen elements, opening new modification options,

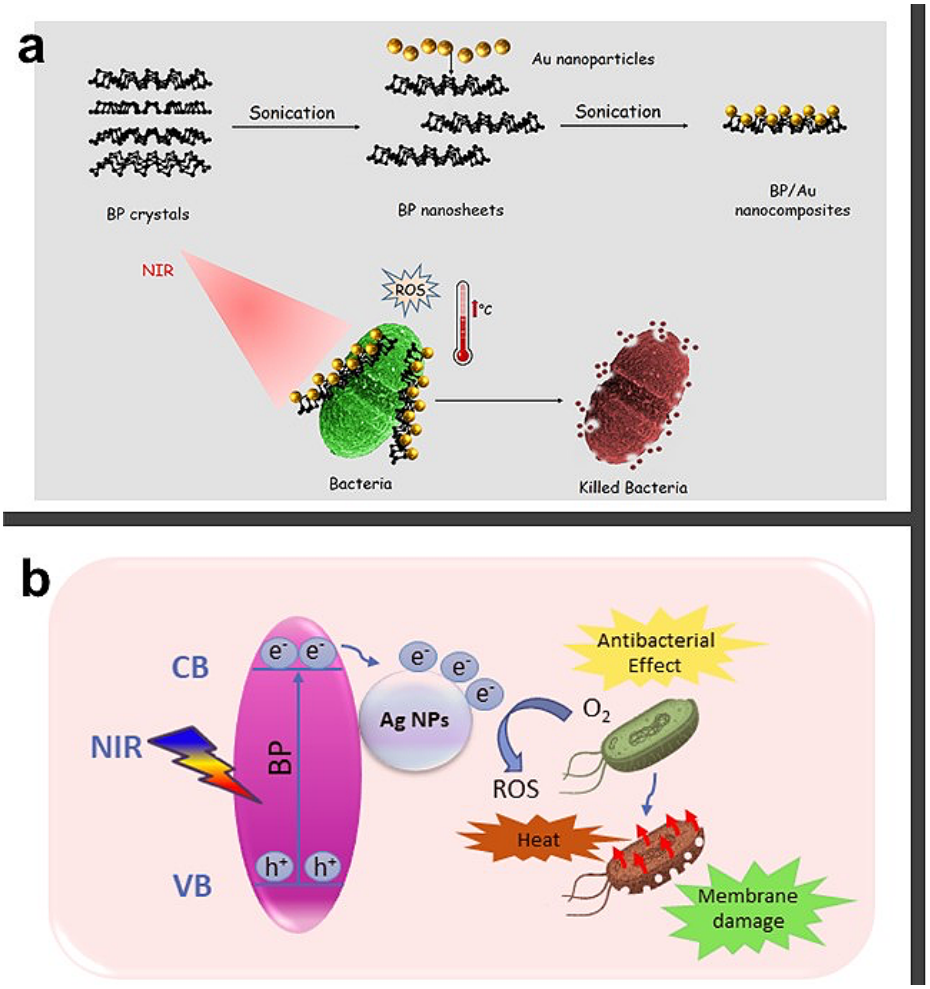

Figure 9. Proposed mechanism of (a) BP/Au. Reprinted (adapted) with permission from [62]. Copyright 2020 American Chemical Society. (b) BP/Ag for photothermal therapy. Reproduced with permission.[63] Copyright 2022, Wiley.

such as thermal treatment. We also present the development of three distinct g-CN-based photocatalysts through vacancy engineering.[58] The investigation focused on their photophysical and morphological properties, along with their improved photocatalytic performance. By subjecting g-CN to post-annealing at different temperatures (610, 630, and 650 °C), we achieved the formation of more porous, thin-layered, and higher surface area g-CN with increasing temperature. Additionally, the introduction of *N*-vacancy in g-CN led to remarkable photophysical properties, revealing the emergence of new mid-gap states among the band energy levels. Out of these photocatalysts, the g-CN annealed at 650 °C (A-g-CN_{650}) demonstrated the highest photocatalytic activity in the oxidative Mannich reaction. It achieved an impressive conversion rate of 98% within just 2 hours, significantly faster than other reaction kinetics previously reported. Furthermore, the A-g-CN-catalyzed photooxidative Mannich-type reaction was examined with various nucleophiles, such as nitromethane, primary, and secondary alcohols, showing enhanced C–C formation compared to pristine g-CN. This enhancement is attributed to its superior visible light absorption capacity, excellent high surface area, and enhanced separation of photogenerated charge carriers. We continued our research with guanidine-based g-CN by treating at three different temperatures (450, 500, and 550 °C).[59] The effect of polycondensation temperature on the structure of heptazine units has remarkably changed the photocatalytic performance on NO photooxidation. g-CN synthesized at 500 °C (g-CN500) exhibited the best photocatalytic performance, making it the ideal candidate for anchoring with 8.0 ± 0.5 wt.% Fe_3O_4 NPs. This innovative approach resulted in a photocatalyst Fe_3O_4/ g-CN500 having even higher activity and selectivity towards solid-state NO_x oxidation and storage under visible light irradiation.

The usage of stable inorganic semiconductor material, BP was extended further on developing efficient and that can absorb a broad range of solar wavelengths to trigger

various photochemical processes is highly appealing.[60] One of them was using BP as a photocatalyst and onium salts as co initiators to initiate the polymerization of different monomers using visible and near-infrared (NIR) light. When exposed to light, few-layer BP generates excited electrons and holes, which then participate in electron transfer reactions with onium salts. These reactions lead to the formation of free radicals capable of initiating free radical polymerization. Among the tested onium salts, aryldiazonium salt proved to be the most efficient in the photopolymerization process, primarily due to its favorable reduction potential when coupled with the conduction edge potential of BP. This innovative approach also opens up possibilities for the *in situ* preparation of composite materials composed of BP and polymers.

The development of photoinduced copper-catalyzed azide-alkyne click (CuAAC) reaction routes that can work with long-wavelength light is highly appealing in the fields of organic and polymer chemistry. In a follow-up study, we introduce a new synthetic approach for the photoinduced CuAAC reaction using BPNs as photocatalysts and they were exposed to white LED and near-infrared (NIR) light during the reaction.[61] Under light irradiation, the BPNs generated excited electrons in its conduction band (CB) and holes in its valence band (VB). These excited electrons were transferred to Cu (II) ions, leading to the production of active Cu (I) catalyst. The ability of BPNs to initiate the CuAAC reaction was explored by studying the reaction between various alkyne and azide derivatives under both white LED and NIR light irradiation. The use of NIR light allowed for deeper penetration, enabling the synthesis of diverse macromolecular structures, including functional polymers, cross-linked networks, and block copolymers. The intermediates and final products were thoroughly characterized using spectral and chromatographic analyses to evaluate their structural and molecular properties.

The utilization of photocatalysis has garnered prominence in bio-applications, notably in the domains of photothermal therapy and photodynamic therapy. Photothermal therapy exploits light-absorbing agents to transduce light energy into thermal energy, precisely directing its effects towards cancer cells or distinct tissues through controlled hyperthermia induction. In contradistinction, photodynamic therapy employs photosensitive compounds and light to initiate a photochemical reaction, instigating the production of reactive oxygen species that differentially dismantle aberrant cells or pathogens, while concurrently safeguarding the integrity of neighboring healthy tissue.[62] The BP nanosheets and BP/Au nanocomposites have been shown to possess effective antibacterial and antibiofilm properties when exposed to NIR light.[63] The inherent photothermal effect, nanoknife effect, and oxidative stress activity of BP/Au nanocomposites lead to bacterial morphological defects and cell death. The antibacterial efficacy was confirmed through various methods, including the photothermal effect, bacterial growth curve, colony counting, GSH depletion assay, live/dead fluorescence staining, and scanning electron microscopy (SEM). While BP nanosheets alone, with or without NIR light, were not able to completely eliminate the bacteria, BP/Au nanocomposites exposed to NIR light successfully eradicated all bacteria by destroying the bacterial cell membranes (**Figure 9a**). Additionally, the antibiofilm activities of both BP nanosheets and BP/Au nanocomposites were investigated, and it was found that the nanocomposites reduced the biofilm formation of E. faecalis by up to 58%. This research presents a new and promising approach for combatting pathogenic bacteria and lays

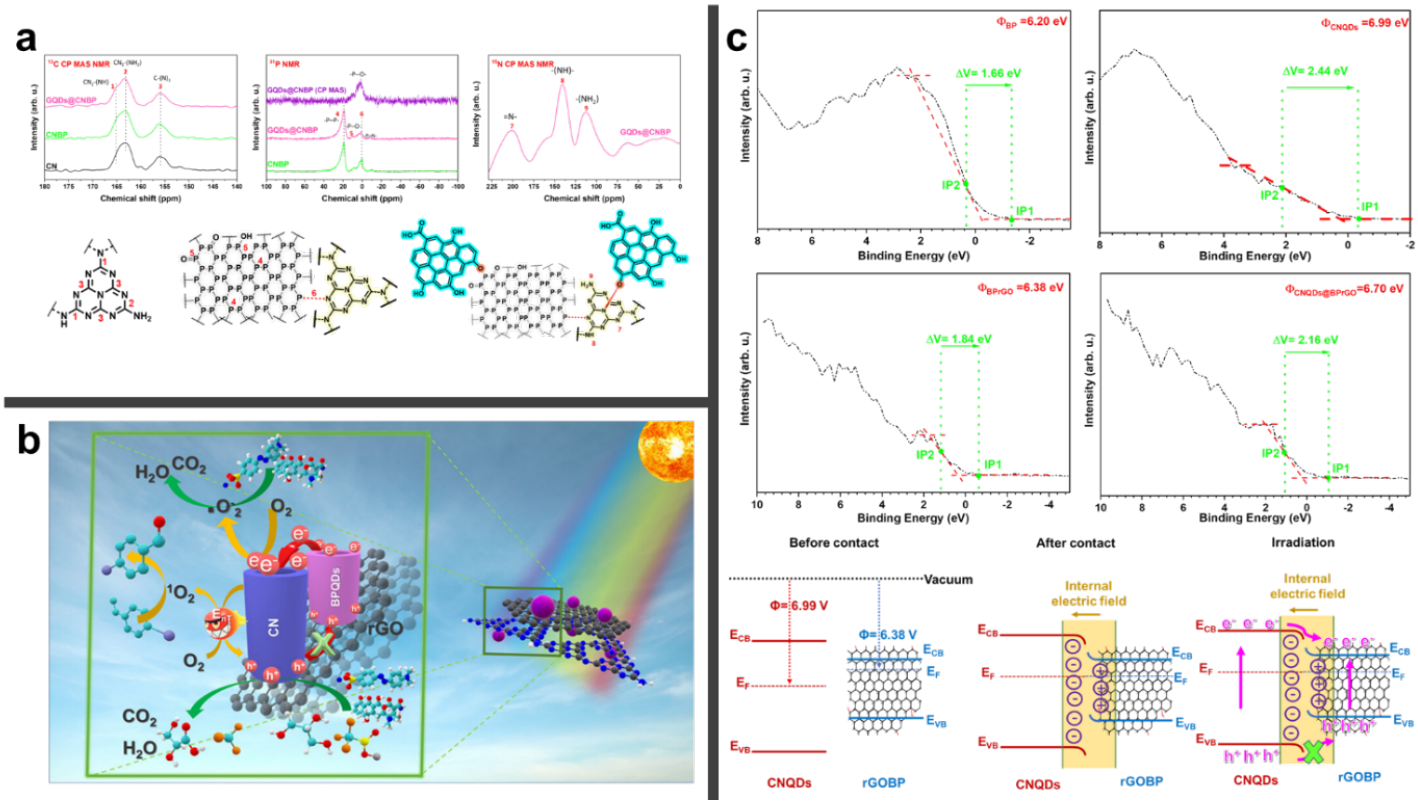

Figure 10. (a) Internal interaction between GQDs, gCN and BP for superior photodegradation performance,[65] (b) Proposed mechanism of BPQDs/GCN-rGO for photooxidation reactions,[66] (c) The work functions of BP, CNQDs, rGOBP, CNQDs@rGOBP and internal electric field (IEF) between semiconductors, before, after contact and under irradiation, respectively, and the obtained bending of band edges for rGOBP, and CNQDs. Reprinted from [67], Copyright 2023, with permission from Elsevier.

the foundation for the future development of innovative platforms to fight against bacterial infections. In this study, we developed a new type of nanocomposite using BP nanosheets and silver (Ag) NPs that can be activated by NIR light.[64] This composite demonstrated improved antibacterial properties compared to using BP nanosheets alone. The enhanced antibacterial effects were achieved by inhibiting bacterial growth, raising the surrounding temperature, and producing reactive oxygen species when exposed to NIR light. The nanocomposites showed higher antibacterial efficiency against certain types of bacteria, specifically Gram-positive ones, compared to Gram-negative bacteria (**Figure 9b**). Different tests, such as agar plate assays, Live/dead fluorescence staining, and the oxidation of GSH test, confirmed that NIR light boosts the antibacterial performance of both BP nanosheets and BP/Ag nanocomposites. The findings suggest that these NIR-light-driven BP-based nanocomposites could be viable alternatives to antibiotics for antibacterial applications. Moreover, their ability to perform effectively under NIR light offers potential for various applications, including biofilm, wound, and cancer therapy.

In recent years, we started a series of photodegradations of organic pollutants from wastewater using metal-free ternary heterojunctions. Ternary heterojunctions represent a fascinating and promising class of materials in the realm of semiconductor physics and nanotechnology.[65] These structures involve the strategic integration of three distinct semiconductor materials, each possessing unique electronic and optical properties. Ternary heterojunctions offer a rich playground for tailoring material interfaces, band alignments, and charge transport characteristics, thereby enabling a diverse range of applications. As researchers delve deeper into the synthesis, characterization, and theoretical understanding of ternary heterojunctions, they pave the way for innovative breakthroughs that have the potential to redefine the landscape of modern semiconductor technology.[66] We successfully created CNQDs@rGOBP ternary heterojunctions using elements C, N, O, and P, which are abundant in nature.[67]the state-of-the-art photocatalytic systems for various applications have not yet reached the desired level due to poor visible-light absorption and the high-cost requirements of the developed photocatalysts. Recently, the combination of different semiconductors via band engineering has been regarded as a highly efficient strategy to construct metal-free photocatalysts. In this study, a novel ternary heterojunction photocatalyst was fabricated by decorating reduced graphene oxide/black phosphorus binary heterojunctions (rGOBP We employed advanced instrumental techniques to characterize these heterojunctions. The interaction between CNQDs and rGOBP at the interfaces led to a heterojunction with excellent photophysical properties. We tested the photocatalysts for degrading methyl orange (MO) and found that the combination of CNQDs and rGOBP resulted in superior performance compared to using them individually. When the components were combined in aqueous media, the degradation efficiency of organic pollutants was 2.5 times higher than using the materials separately. The photocatalytic activity was attributed to a nonclassical type-I heterojunction, and the researchers also studied the band potentials and charge flow at the interfaces. The strong interaction among the components and structural matching enhanced the chemical stability of BP. Overall, CNQDs@rGOBP offers a sustainable and metal-free photocatalyst with controllable band potentials and high charge separation properties, making it a promising option for eco-friendly photocatalysts (**Figure 10c**). Furthermore, we introduced another novel and effective photocatalyst called GQDs@CNBP, which exhibited exceptional performance and stability for degrading organic pollutants in water under visible light.[68] Using advanced techniques like XRD, FTIR, XPS, and ssNMR analyses, we studied the structure-activity relationship of the heterojunction. The results revealed strong connections between CN and BP through P–N bonds, with GQDs' polar functional groups attached to P–O in BP and N–O in CN on the CNBP surface (**Figure 10a**). This ternary heterojunction demonstrated significant coupling at the interfaces, leading to enhanced photophysical properties. It outperformed pristine components and similar photocatalysts reported in the literature for degrading MO and tetracycline (TC). We also confirmed a photogenerated charge migration pathway and proposed a photodegradation mechanism based on the band alignments of the ternary structure. We identified GQDs@CNBP as a complex-type-II heterojunction, involving the farthest charges on the band edges. Notably, GQDs@CNBP achieved photooxidation of glucose using only water as a solvent and no additional agents, indicating efficient charge separation and stability. Besides, we expanded the scope of BPQDs/CN-rGO, as a metal-free photocatalyst with remarkable abilities for various organic transformations using a photooxidation mechanism.[69] By optimizing the contents of individual components in binary and ternary heterojunctions, we discovered synergistic interactions that significantly improved photocatalytic performance. The ternary heterojunction demonstrated superior efficiency in degrading MO and TC, with reaction kinetics of 0.1289 and 0.0335 min^{-1} respectively. Experimental measurements of Fermi levels confirmed the nonclassical-type-II heterojunction of BPQDs/CN-rGO. The photocatalyst was found to facilitate different organic transformations, generating key reactive species like $O_2^{\bullet-}$, h^+, and $^1O_2$. Notably, it selectively converted glycerol to glyceric acid (45%) and styrene to benzaldehyde derivatives (40%) and also enabled the generation of $\bullet CF_3$ radicals from the Langlois reagent, where h^+ played an essential role (**Figure 10b**). We anticipate that the ternary heterojunction, BPQDs/CN-rGO, will find extensive applications in various conditions and contexts.

Conclusion and Future Outlook

In this article, we highlighted our research group's studies about the synthesis and catalysis of monodisperse transition metal NPs, non-metallic 2D semiconductor materials and their nanocomposites for various applications including the hydrogen generation from the chemical hydrogen storage materials, sustainable organic transformations, pollutant degradation from water and photoredox C-H functionalization. There are many synthesis protocols available for the synthesis of transition metal NPs, but a minority of them provides size, shape, and composition-controlled synthesis of high quality/monodisperse NPs, which glows our synthesis strategy described above as a preferable one. Although we reported many successful syntheses of mono/bimetallic NPs, the synthesis of monodisperse transition metal NPs is very challenging due to the number of parameters that must be optimized requiring chemical and time waste. Moreover, most of the current synthesis protocols result in low yield of monodisperse NPs. In this respect, we believe that artificial intelligence/machine learning should be integrated to the synthesis of transition metal NPs and recipe optimization on the way to sustainable chemistry. As we highlighted above, another way to develop more sustainable catalysts might be the use of non-metallic 2D semiconductor materials as photocatalysts for various chemical transformations under sunlight irradiation. In this regard, the studies on the rational design of heterojunction photocatalysts including different 0D/2D/3D semiconductor materials as well as the non-precious metal NPs should be continued.

References

1 D. Rodríguez-Padrón, A. R. Puente-Santiago, A. M. Balu, M. J. Muñoz-Batista and R. Luque, *ChemCatChem*, 2019, **11**, 18–38.
2 J. R. Ludwig and C. S. Schindler, *Chem*, 2017, **2**, 313–316.
3 G. Centi and S. Perathoner, *Catal. Today*, 2008, **138**, 69–76.
4 D. S. Su, J. Zhang, B. Frank, A. Thomas, X. Wang, J. Paraknowitsch and R. Schlögl, *ChemSusChem*, 2010, **3**, 169–180.
5 C. M. Friend and B. Xu, *Acc. Chem. Res.*, 2017, **50**, 517–521.
6 C. Descorme, P. Gallezot, C. Geantet and C. George, *ChemCatChem*, 2012, **4**, 1897–1906.
7 M. Heitbaum, F. Glorius and I. Escher, *Angew. Chemie Int. Ed.*, 2006, **45**, 4732–4762.
8 L. D. Pachón and G. Rothenberg, *Appl. Organomet. Chem.*, 2008, **22**, 288–299.
9 S. Drummer, T. Madzimbamuto and M. Chowdhury, *Materials (Basel).*, 2021, **14**, 2700.
10 N. Yan, C. Xiao and Y. Kou, *Coord. Chem. Rev.*, 2010, **254**, 1179–1218.
11 D. Astruc, *Nanoparticles Catal.*, 2008, 1–640.
12 A. K. Singh and Q. Xu, *ChemCatChem*, 2013, **5**, 652–676.
13 N. Eom, M. E. Messing, J. Johansson and K. Deppert, *ACS Nano*, 2021, **15**, 8883–8895.
14 J. E. S. van der Hoeven, J. Jelic, L. A. Olthof, G. Totarella, R. J. A. van Dijk-Moes, J. M. Krafft, C. Louis, F. Studt, A. van Blaaderen and P. E. de Jongh, *Nat. Mater. 2021 209*, 2021, **20**, 1216–1220.
15 C. Wang, Y. Shi, D. Qin and Y. Xia, *Nanoscale Horizons*, 2023, **8**, 1194–1204.
16 Ö. Metin, V. Mazumder, S. Özkar and S. Sun, *J. Am. Chem. Soc.*, 2010, **132**, 1468–1469.
17 Ö. Metin, S. Özkar and S. Sun, *Nano Res.*, 2010, **3**, 676–684.
18 Ö. Metin, S. F. Ho, C. Alp, H. Can, M. N. Mankin, M. S. Gültekin, M. Chi and S. Sun, *Nano Res.*, 2013, **6**, 10–18.
19 H. Kilic, M. Turgut, M. S. Yilmaz, O. Dalkilic and Ö. Metin, *ACS Sustain. Chem. Eng.*, 2018, **6**, 11433–11440.
20 Ö. Metin, E. Kayhan, S. Özkar and J. J. Schneider, *Int. J. Hydrogen Energy*, 2012, **37**, 8161–8169.
21 H. Can and Ö. Metin, *Appl. Catal. B Environ.*, 2012, **125**, 304–310.
22 D. Sun, V. Mazumder, Ö. Metin and S. Sun, *ACS Nano*, 2011, **5**, 6458–6464.
23 H. Göksu, H. Can, K. Şendil, M. S. Gültekin and Ö. Metin, *Appl. Catal. A Gen.*, 2014, **488**, 176–182.
24 S. Diyarbakir, H. Can and Ö. Metin, *ACS Appl. Mater. Interfaces*, 2015, **7**, 3199–3206.
25 H. Göksu, S. F. Ho, Ö. Metin, K. Korkmaz, A. Mendoza Garcia, M. S. Gültekin and S. Sun, *ACS Catal.*, 2014, **4**, 1777–1782.
26 S. Pal, Ö. Metin and Y. E. Türkmen, *ACS Omega*, 2017, **2**, 8689–8696.
27 R. C. P. Oliveira, M. Sevim, B. Šljukić, C. A. C. Sequeira, Ö. Metin and D. M. F. Santos, *Catal. Today*, 2020, **357**, 291–301.
28 S. B. Kalidindi, M. Indirani and B. R. Jagirdar, *Inorg. Chem.*, 2008, **47**, 7424–7429.
29 H. Wu, Y. Cheng, Y. Fan, X. Lu, L. Li, B. Liu, B. Li and S. Lu, *Int. J. Hydrogen Energy*, 2020, **45**, 30325–30340.
30 U. Sanyal, U. B. Demirci, B. R. Jagirdar and P. Miele, *ChemSusChem*, 2011, **4**, 1731–1739.
31 G. Rothenberg, *Catalysis: Concepts and Green Applications*, 2008.
32 Ö. Metin, A. Mendoza-Garcia, D. Dalmizrak, M. S. Gültekin and S. Sun, *Catal. Sci. Technol.*, 2016, **6**, 6137–6143.
33 Ö. Metin, H. Can, K. Şendil and M. S. Gültekin, *J. Colloid Interface Sci.*, 2017, **498**, 378–386.
34 F. Sordello, P. Calza, C. Minero, S. Malato and M. Minella, *Catalysts*, 2022, **12**, 1–21.
35 W.-J. Ong, L.-L. Tan, Y. H. Ng, S.-T. Yong and S.-P. Chai, *Chem. Rev.*, 2016, **116**, 7159–7329.
36 H. Kahri, M. Sevim and Ö. Metin, *Nano Res.*, 2017, **10**, 1627–1640.
37 M. Aksoy and Ö. Metin, *ACS Appl. Nano Mater.*, 2020, **3**, 6836–6846.
38 M. Aksoy, S. E. Korkut and Ö. Metin, *Int. J. Hydrogen Energy*, 2023, **48**, 22921–22933.
39 B. Verhoeven, in *EVS 2017 - 30th International Electric Vehicle Symposium and Exhibition*, American Chemical Society, 2017, vol. 2, pp. 188–195.
40 O. Altan and Ö. Metin, *Appl. Surf. Sci.*, 2021, **535**, 147740.
41 O. Altan, E. Altintas, S. Alemdar and Ö. Metin, *Chem. Eng. J.*, 2022, **441**, 136047.
42 K. Maeda, *J. Photochem. Photobiol. C Photochem. Rev.*, 2011, 12, 237–268.
43 G. Yanalak, F. Doganay, Z. Eroglu, H. Kucukkececi, E. Aslan, M. Ozmen, S. Z. Bas, O. Metin and I. Hatay Patir, *Appl. Surf. Sci.*, 2021, **557**, 149755.
44 S. Yılmaz, E. G. Acar, G. Yanalak, E. Aslan, M. Kılıç, İ. Hatay Patır and Ö. Metin, *Appl. Surf. Sci.*, 2022, **593**, 153398.
45 G. Yanalak, S. Yılmaz, Z. Eroglu, E. Aslan, O. Metin and I. H. Patir, *Int. J. Energy Res.*, 2022, **46**, 17189–17203.
46 E. Aslan, Z. Eroğlu, G. Yanalak, Ö. Metin and I. Hatay Patir, *Appl. Surf. Sci.*, 2022, **604**, 154435.
47 G. Yanalak, Z. Eroglu, S. Yılmaz, S. Z. Bas, O. Metin and I. H. Patir, *Int. J. Hydrogen Energy*, 2023, **48**, 14238–14254.
48 E. G. Acar, S. Yılmaz, Z. Eroglu, İ. A. Çekceoğlu, E. Aslan, İ. H. Patır and O. Metin, *Catalysts*, 2023, **13**, 1006.
49 E. G. Acar, S. Yılmaz, Z. Eroglu, E. Aslan, Ö. Metin and I. H. Patır, *J. Alloys Compd.*, 2023, **950**, 169753.
50 F. X. Felpin and S. Sengupta, *Chem. Soc. Rev.*, 2019, 48, 1150–1193.
51 X. Zhang, Y. Mei, Y. Li, J. Hu, D. Huang and Y. Bi, *Asian J. Org. Chem.*, 2021, 10, 453–463.
52 X. Y. Yu, J. R. Chen and W. J. Xiao, *Chem. Rev.*, 2021, 121, 506–561.
53 S. S. Babu, P. Muthuraja, P. Yadav and P. Gopinath, *Adv. Synth. Catal.*, 2021, 363, 1782–1809.
54 D. Koziakov, G. Wu and A. Jacobi Von Wangelin, *Org. Biomol. Chem.*, 2018, 16, 4942–4953.
55 E. Kalay, H. Seyin Kü Çü Kkeçeci, H. Kilic, O. ¨ Nder Metin, R. Li, / Chemcomm and C. Communication, *Chem. Commun.*, 2020, **56**, 5901–5904.
56 Z. Eroglu, M. S. Ozer, T. Kubanaliev, H. Kilic and Ö. Metin, *Catal. Sci. Technol.*, 2022, **12**, 5379–5389.
57 M. S. Ozer, Z. Eroglu, A. S. Yalin, M. Kılıç, U. Rothlisberger and O. Metin, *Appl. Catal. B Environ.*, 2022, **304**, 120957.
58 T. Kubanaliev, Z. Eroglu, M. S. Ozer and Ö. Metin, *Catal. Sci. Technol.*, 2023, **13**, 2317–2329.
59 M. Irfan, M. Sevim, Y. Koçak, M. Balci, Ö. Metin and E. Ozensoy, *Appl. Catal. B Environ.*, 2019, **249**, 126–137.
60 A. Kocaarslan, Z. Eroglu, G. Yilmaz, O. Metin and Y. Yagci, *ACS Macro Lett.*, 2021, **10**, 679–683.
61 A. Kocaarslan, Z. Eroglu, Ö. Metin and Y. Yagci, *Beilstein J. Org. Chem. 17164*, 2021, **17**, 2477–2487.
62 J. R. Choi, K. W. Yong, J. Y. Choi, A. Nilghaz, Y. Lin, J. Xu and X. Lu, *Theranostics*, 2018, **8**, 1005–1026.
63 İ. Aksoy, H. Küçükkeçeci, F. Sevgi, Ö. Metin and I. Hatay Patir, *ACS Appl. Mater. Interfaces*, 2020, **12**, 26822–26831.
64 İ. A. Çekceoğlu, Z. Eroglu, H. Küçükkeçeci, F. Sevgi, M. Ersoz, I. H. Patir and Ö. Metin, *ChemistrySelect*, 2022, **7**, e202104137.
65 H. Wang, L. Zhang, Z. Chen, J. Hu, S. Li, Z. Wang, J. Liu and X. Wang, *Chem. Soc. Rev.*, 2014, **43**, 5234–5244.
66 J. Low, J. Yu, M. Jaroniec, S. Wageh, A. A. Al-Ghamdi J X Low, J. G. Yu, S. Wageh, A. A. Al-Ghamdi and M. Jaroniec, *Adv. Mater.*, 2017, **29**, 1601694.
67 Z. Eroglu, B. Sündü and O. Metin, *Mater. Today Sustain.*, 2023, **23**, 100418.
68 Z. Eroglu and O. Metin, *ACS Appl. Nano Mater.*, 2023, **6**, 7960–7974.
69 Z. Eroglu, M. S. Ozer and O. Metin, *ACS Sustain. Chem. Eng.*, 2023, **11**, 7560–7572.